## Demonstration of $3\pm0.12\,dB$ power splitting over 145 nm optical bandwidth in a 31- $\mu$ m long 3-dB rapid adiabatic coupler

Josep M. Fargas Cabanillas\*, Bohan Zhang and Miloš A. Popović†

Department of Electrical and Computer Engineering, Boston University, 8 St. Mary's Street, Boston, MA 02215, USA \*jofa@bu.edu, †mpopovic@bu.edu

**Abstract:** We experimentally validate the rapid adiabatic coupling (RAC) concept and demonstrate  $50\pm1.4\%$  ( $3\pm0.12$  dB) power splitting over a record 145 nm bandwidth from either port of a  $31\mu$ m-long,  $2\times2$  coupler, the widest  $\pm1.4\%$ -bandwidth by a factor of 4. © 2020 The authors.

The complexity and capabilities of silicon photonic circuits on chip are rapidly advancing, especially as electronic control is being integrated. Recent demonstrations include systems-on-chip with monolithically integrated, wavelength-division multiplexed, microring-based optical I/O including microprocessors [1, 8], large-scale optical phased arrays [3], linear-optical photonic signal processing based on Mach-Zehnder arrays [4], and a two-qubit quantum processor [2]. 3 dB directional couplers are fundamental building blocks of integrated photonic circuits, and are desired to be low-loss, broadband with precise splitting ratio, compact and fabrication tolerant. These metrics determine the performance of Mach-Zehnder interformeters, switches and modulators, and impact complex circuits comprising many cascaded devices such as reconfigurable processors or switch matrices [4, 17]. Conventional approaches including synchronous, adiabatic, and multimode interference couplers trade off size and bandwidth/splitting ratio.

In this paper, we experimentally demonstrate record performance from a  $2\times2$  3-dB coupler based on a recently proposed concept we call a rapid adiabatic coupler (RAC) [9,18]. It provides the short lengths of synchronous couplers along with the broadband and tolerant performance of adiabatic couplers. We show experimentally RACs with better than  $50\% \pm 1.4\%$  splitting ratio over a 145 nm optical bandwidth, well outperforming all coupler designs to date, in a compact 31  $\mu$ m length that may enable substantial performance improvements in aforementioned photonic circuits.

We proposed rapid adiabatic coupling (RAC) [9] as a design technique that builds on the theory of adiabatic photonic device design, but takes advantage of thus far unused degrees of freedom that are particularly relevant in high index contrast. Conventional adiabatic 3 dB couplers are robust and broadband, but long. They usually exceed  $100 \,\mu m$  even for optimized tapering designs that smooth out the coupling-to-asynchronism ( $\kappa/\delta\beta$ ) ratio along the structure. Simple synchronous directional couplers, on the other hand, provide minimal lengths but are narrowband and sensitive to variations. Rapid adiabatic couplers are adiabatic devices that can provide low crosstalk in a much shorter length (in some cases  $\sim 10 \times$  shorter). Whereas in conventional adiabatic couplers one may minimize coupling by optimizing tapering along the length, in a RAC device we also use transverse bending of the geometry to exactly zero out the dominant coupling mechanism, here the coupling between the symmetric and antisymmetric modes [9]. Our first experimental report of RAC coupler performance showed  $3\pm 0.3 dB$  splitting over 130 nm bandwidth with a length of  $31\mu m$  [18]. The device was designed for TE polarization, but performance characterization was limited by spurious

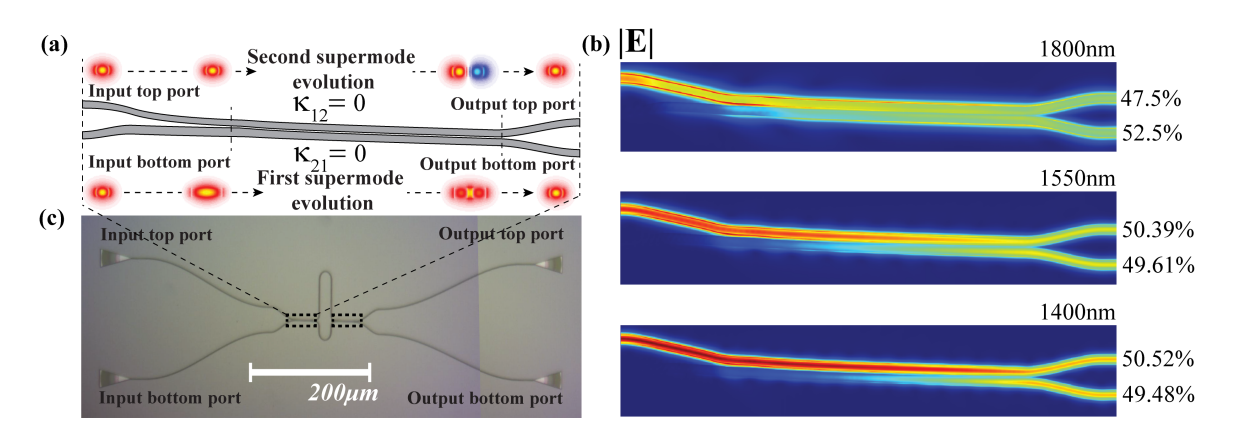


Fig. 1: (a) RAC schematic.(b) 3D FDTD simulations of the device at different wavelengths.(c) Optical micrograph of the Mach Zehnder Interferometer (MZI) measured to test the RAC. Both dashed black lines boxes include the same RAC showed on (a).

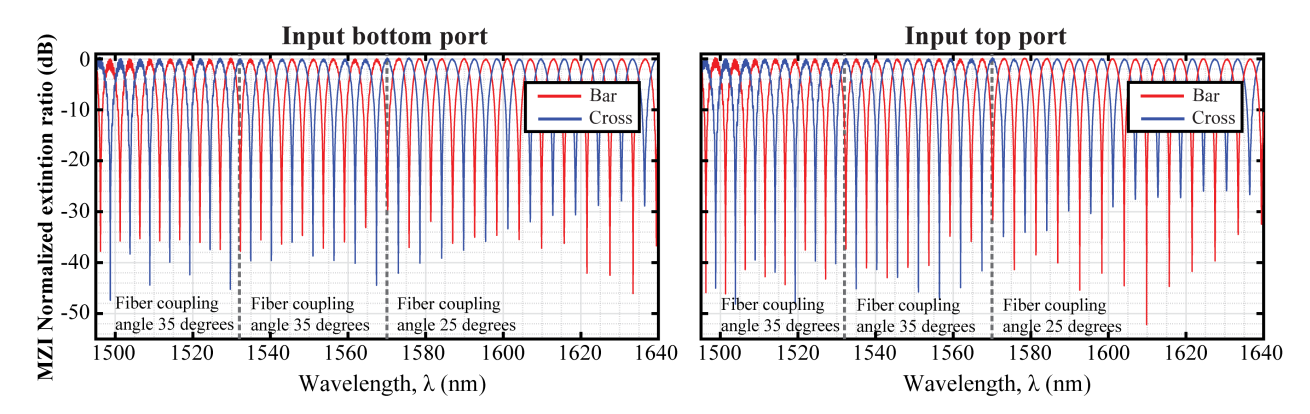


Fig. 2: Measured bar- and cross-port transmission responses of a Mach-Zehnder interferometer comprising two RAC couplers, whose extinction ratio indicates the splitting ratio of the coupler. The two vertical dashed lines indicate three separate measurements. Input polarization state was not changed during the measurements.

low-level TM polarization excitation in the fiber-to-chip edge couplers. To demonstrate the device's capabilities, a chip redesign using grating couplers, which are highly polarization selective, was fabricated, allowing us to characterize the splitting ratio through high extinction measurements and substantiate the record predicted performance experimentally. We also obtain an upper bound to the coupler's insertion loss which was not previously characterized.

Fig. 1(a) depicts the device geometry, and shows the evolution of the fundamental and the second-order supermodes along the structure. The waveguide port separation is  $1.2\mu$ m. The *input bottom port* starts with a standard single-mode bus waveguide width and tapers out to a wider width at the entrance to the coupling region. The *input top port* also starts with the single-mode width but tapers to a narrower waveguide. The widths then remain constant as the gap decreases to the coupling region gap (100 nm). In the coupling region, the gap remains constant while the two waveguides change their width until both have the same output width, similar to a conventional adiabatic coupler. One of the key concepts of the RAC design is that the structure also bends in the transverse direction [see curved coupling region in Fig. 1(a)] to precisely zero out the coupling ( $\kappa_{12}$  and  $\kappa_{21}$ ) by canceling contributions from the four sidewalls [9, 18]. This allows a drastic reduction in length, since the dominant coupling is now the next closest mode in propagation constant (a considerably larger  $\delta\beta$ ). At the output, the waveguides split symmetrically while increasing the waveguide width back to the bus waveguide width.

Fig 1(b) shows the electric field time-average magnitude at three wavelengths across a very large bandwidth. At all three –  $1800 \,\mathrm{nm}$ ,  $1550 \,\mathrm{nm}$  and  $1400 \,\mathrm{nm}$  – simulations show a splitting ratio very close to 3 dB. To our knowledge, this is the first demonstration of a  $31 \,\mu\mathrm{m}$  long device showing such a precise splitting ratio over such wide bandwidth.

Fig. 1(c) shows the imbalanced Mach-Zehnder interferometer (MZI) used to measure the splitting ratio. Test devices were fabricated using electron beam lithography on a 220 nm silicon-on-insulator (SOI) wafer. Fig. 2 shows the extinction ratio for bar- and cross-port transmission for each of the two input ports. The bar transmission extinction ratio is used to extract the splitting ratio.

The normalized splitting ratio, plotted in Fig. 3(a), is extracted (assuming the difference in losses between the two MZI arms is negligible) for each input port. The coupler shows a splitting ratio of  $3\pm0.12$ dB ( $50\pm1.4\%$ ) over a 145 nm optical bandwidth. The device is 31  $\mu$ m long, and the coupling region itself is only  $18\mu$ m long. We used a set of cascaded balanced MZIs to characterize the loss per coupler. An example optical micrograph of such devices is shown in Fig. 3(a) here with 18 RAC couplers per structure. We designed 3 sets of structures – with 18, 42, and 78 cascaded RACs respectively – from which we estimate the device insertion loss. For each structure set, we designed two structures with the same number of RACs, one to characterize loss when exciting each of the two input ports. Fig. 3(c) shows insertion loss vs. wavelength obtained from linear fits at each wavelength of the loss for the three cascades. The measurement upperbounds the insertion loss per device at 0.4–0.5 dB. This considerably exceeds the simulated insertion losses shown also in the plot, of below 0.1 dB. We are investigating the reasons for the discrepancy, and believe that phase errors permitted in our characterization geometry may be the culprit. We expect device performance to reach close to the simulated values since severe departures from the intended shape would also have had deleterious effects on the splitting ratio, which we do not observe.

In Fig. 3(d) we survey the state of the art results in literature by revisiting the plot in [18], showing bandwidth over which a given splitting ratio is achieved, and device length. The plot is revised for the new splitting performance con-

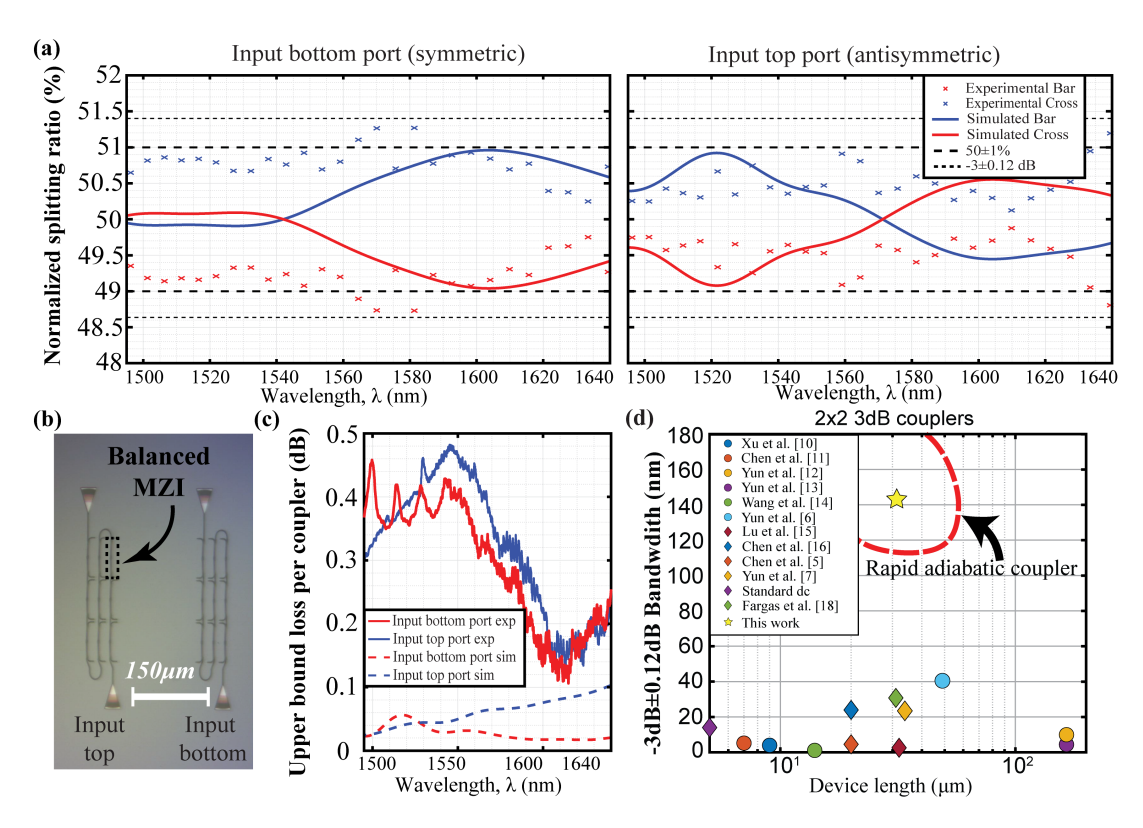


Fig. 3: (a) Experimental and simulated normalized splitting ratio for both input ports; (b) optical micrograph of a cascade of balanced MZIs with 18 RACs to measure insertion loss; (c) insertion loss per coupler, simulated and experimentally extracted from linear fit to loss from 18, 42, and 78 cascaded devices; (d) summary of 3 dB couplers reported in literature [5–7, 10–16, 18]. Values have been extracted from the splitting ratios reported.

dition of  $3\pm0.12$ dB or better. This places all other state of the art couplers on the bottom of the plot and highlights the performance improvement demonstrated in the present work. The  $31\mu$ m device length includes input/output regions.

The measured results validate the rapid adiabatic coupling design technique as a way to realize compact, efficient devices with the best properties of adiabatic devices, without their excessive size. We believe it should find ready application in integrated photonics for MZI modulators, linear optics quantum computing circuits, neuromorphic photonics, reconfigurable integrated waveguide meshes and switches, and others.

Acknowledgments: This work was funded in part by NSF EQuIP program grant #1842692. Chips were fabricated by Applied Nanotools, Inc.

## References

- 1. M. Wade et al. "Monolithically Integrated Electronics-Photonics", European Conference on Optical Communication, Rome, pp. 1-3. (2018).
- 2. Qiang X. et al. "Large-scale silicon quantum photonics implementing arbitrary...", Nature Photonics, Vol. 12, pages 534—539 (2018).
- 3. J. Sun et al. "Dense integration", Nature, Vol. 493, page 195 (2013).
- 4. Y. Shen et al. "Deep learning with coherent nanophotonic circuits", Nature Photonics 11, page 441 (2017).
- 5. Chen, George F. R. et al. "Broadband Silicon-On-Insulator directional couplers using...", Scientific Reports, 7 2045-2322 (2017).
- 6. Yun, H.et al. "Broadband 2x2 adiabatic 3dB coupler using silicon-on-insulator sub-wavelength...", Opt. Lett. 41, 3041–3044 (2016).
- 7. Yun, H. et al. "Ultra-broadband 2x2 adiabatic 3 dB coupler using subwavelength-grating-assistred...", Opt. Lett. 43, 1935-1938 (2018).
- 8. Chen S. et al. "Single-chip microprocessor that communicates directly using light", Nature 528,534-538 (2015)
- 9. Fargas Cabanillas J. M. et al. "Fast adiabatic mode evolution based on..." CLEO: 2018 OSA Technical Digest, paper STh4A.2. (2018).
- 10. Xu, D.-X. et al. "High bandwidth SOI photonic wire ring resonators using MMI..." Opt. Express 15, 3149-3155 (2007).
- 11. Chen, S. et al. "Compact Dense Wavelength-Division (De)multiplexer Utilizing...", J. Lightwave. Technol. 33, 2279–2285 (2015).
- 12. Yun, H. et al. "2x2 adiabatic 3-dB coupler on silicon-on-insulator rib waveguides...", Photonics North 2013, 89150V-89150V (2013).
- 13. Yun, H. et al. "2x2 Broadband Adiabatic 3-dB Couplers on SOI..." CLEO: 2015 OSA Science and Innovations, paper ST1F.8. (2015).
- 14. Wang, Y. et al. "Compact Broadband Directional Couplers Using Subwavelength Gratings", IEEE Photon. J. 8, 1–8 (2016).
- 15. Lu, Z. et al. "Broadband silicon photonic directional coupler using asymmetric-waveguide...", Opt. Express 23, 3795–3808 (2015).
- 16. Chen, S. et al. "Low-loss and broadband 2x2 silicon thermo-optic Mach-Zehnder switch with bent...", Opt. Lett. 41, 836-839 (2016).
- 17. Perez D. et al. "Multipurpose silicon photonics signal processor core", Nature Communications, Vol. 8, 636 (2017).
- 18. Fargas Cabanillas J. M. et al. "Experimental Demonstration of Rapid...", CLEO: 2019 OSA Technical Digest, paper SM3J.5. (2019).